Effects of neutron sources and moderator materials on therapeutic dose delivery to deep-seated lesions in proton accelerator-based boron neutron capture therapy

F. Hiraga

Hokkaido university Faculty of engineering, Kita-13, Nishi-8, Kita-ku, Sapporo, Hokkaido, 060-8628, Japan
tel. +81-11-706-6652, fax. +81-11-706-6652, email: hiraga@eng.hokudai.ac.jp.

Abstract

This study aimed to identify the optimal conditions for delivering sufficient doses to deep-seated lesions within short irradiation times for two boron carriers of different *T*/*N* ratios. The therapeutic depth and irradiation time of a neutron beam for beam shaping assemblies (BSAs) with a Li or Be target and a MgF_2 or CaF_2 moderator were examined with the fast-neutron dose per epithermal neutron (FNR) as a parameter. When $T/N = 3.61$, the therapeutic depth was almost saturated at an FNR of about 10×10^{-13} Gy·cm^2; when the FNR value was about 10×10^{-13} Gy·cm^2, the therapeutic depth of the neutron beam for the BSA with a Be target and a MgF_2 moderator was almost identical to that for the neutron beam for the BSA with a Be target and a CaF_2 moderator, and slightly greater than those for the neutron beams for the BSAs with a Li target and a MgF_2 or CaF_2 moderator; moreover, the irradiation time of the neutron beam for the BSA with a Be target and a MgF_2 moderator was shorter than that for the neutron beam for the BSA with a Be target and a CaF_2 moderator. When $T/N = 100$, the therapeutic depths of the neutron beams for the BSAs varied greatly depending on the FNR, and were greater than the corresponding values for $T/N = 3.61$. We therefore concluded that the BSA with a Be target and a MgF_2 moderator that produced a neutron beam with an FNR of about 10×10^{-13} Gy·cm^2 is optimal for delivering sufficient doses to deep-seated lesions in short irradiation times when $T/N = 3.61$, and stricter control over FNR is required when $T/N = 100$.

Keywords

Proton accelerators; Boron neutron capture therapy; Beam shaping assemblies; Lithium neutron source; Beryllium neutron source; Magnesium fluoride moderator; Calcium fluoride moderator; Dosimetry; Therapeutic depth; Irradiation time

1. Introduction

Beam shaping assemblies (BSAs) for accelerator-based boron neutron capture therapy (AB-BNCT) in which the neutron source is a lithium or beryllium target driven by protons of 2.6 or 30 MeV, respectively, have been commercialized (Neutron Therapeutics, 2016, Sumitomo Heavy Industries, Ltd., 2020). The Li target operates by means of an endothermic $^{7}Li(p,n)^{7}Be$ reaction (Kreiner, 2012), whereas the Be target uses endothermic $^{9}Be(p,xn)$ reactions (Lavelle et al., 2008). Irradiation of a Be target by 30 MeV protons produces more neutrons per kilowatt of proton-beam power than does the irradiation of a Li target by 2.6 MeV protons (Lavelle et al., 2008, Lee and Zhou, 1999). However, the energies of the neutrons emitted from a Li target are less than about 1 MeV. Because a Be target emits neutrons with energies of up to 28 MeV, BSAs with a Be target require filtration methods to reduce the number of neutrons with energies of more than 1 MeV in neutron beams, as detailed below. The differences in the yield and energy of neutrons from Li and Be targets might influence the delivery of a therapeutic dose in AB-BNCT, but this has not been fully clarified.

In BNCT, a high dose of fast neutrons in the neutron beam can lead to undesirable effects, such as damage to irradiated skin; moreover, the dose of γ-rays in the neutron beam is distributed nonselectively to both tumor tissue and large volumes of healthy tissue. Consequently, the International Atomic Energy Agency (IAEA) has recommended that, for clinical irradiation by neutron beams from research reactors, the fast-neutron dose per epithermal neutron (FNR) and the photon dose per epithermal neutron (PHR) should both be less than 2×10^{-13} Gy·cm^2 (IAEA, 2001). However, the application of the target numbers for the FNR and PHR to AB-BNCT should be based on a close examination of the therapeutic dose that is delivered by the BSA. A BSA with a Li target requires a moderator containing fluoride ions to reduce the number of fast neutrons and to enhance the number of epithermal neutrons (0.5 eV < E < 10 keV) in the neutron beam, because fluorine has fairly large cross sections for elastic scattering and for resonance scattering in the energy range 10 keV to 1 MeV. Furthermore, to reduce the number of fast neutrons with energies of more than 1 MeV in the neutron beam, a BSA with a Be target requires fast-neutron filters made of such materials as aluminum, iron, and lead, which have the fairly large cross sections for inelastic scattering, (n,2n), (n,3n) and so on. An investigation of the scattering cross section for moderator materials suggested that a combination of fluoride and aluminum would effectively reduce the number of neutrons with energies in the range 27 keV to 1 MeV (Yonai et al., 2003). The FLUENTAL^{TM} moderator, which contains compressed AlF_3 powder (69%), Al metal (30%), and ^{6}LiF (1%), has been used as a moderator in the design of a BSA (Tahara et al., 2006). However, Monte Carlo calculations to estimate the performance of moderator materials for BSAs with a Li target have shown that to reach a given target number for the ratio of epithermal neutrons to fast neutrons in the neutron beam, the volume of a moderator made of a mixture of AlF_3 (70%) and Al (30%) must be larger than that of a moderator made of MgF_2 (Montagnini et al., 2002). This is because the density of compressed AlF_3 powder [1.85 g·cm^{-3} (Nava and Rosi, 2009)] is lower than that of compressed MgF_2 powder [3.15 g·cm^{-3} (Torres-Sánchez et al., 2021)], suggesting that compact moderators that reduce the number of fast neutrons effectively and that are suitable for hospital installations should be constructed by using compressed MgF_2 powder. Consequently, an experimental BSA with a Li target driven by protons of 2.8 MeV was equipped with an isostatically pressed MgF_2 moderator (Forton et al., 2009).

A compact moderator might also be realized by using crystalline CaF_2, because its density [3.18 g·cm^{-3} (Speziale and Duffy, 2002)] is about the same as that of compressed MgF_2 powder. A BSA with a Be target driven by protons of 30 MeV, constructed for use in clinical trials, was equipped with a series of Pb, Fe, and Al slabs for fast-neutron filtration, in conjunction with a CaF_2 moderator (Tanaka et al., 2009).

However, it is still unclear whether compressed MgF_2 powder or crystalline CaF_2 is optimal for realizing a high-performance compact moderator for AB-BNCT.

BNCT is very effective against certain cancers, such as malignancies of the head or neck (Kato et al., 2004, Aihara et al., 2006, Kankaanranta et al., 2007), or cutaneous melanomas (Fukuda et al., 2003, González et al., 2004). However, to promote the adoption of AB-BNCT, it will be necessary to improve the delivery of a therapeutic dose to deeper-seated cancers such as glioblastoma multiforme, the cells of which infiltrate deeply into the surrounding brain tissue (Chanana et al., 1999). Furthermore, to improve the clinical acceptability of AB-BNCT, the irradiation time by the neutron beam required to deliver adequate doses to deep-seated lesions should be shortened. We have previously examined the effects of the FNR of the neutron beam and the ^{10}B concentrations of tumor tissue and normal tissue on the delivery of therapeutic doses to deep-seated lesions (Hiraga and Ooie, 2019). BSA models with a MgF_2 moderator and a Li target driven by protons of 2.8 MeV, which produced a neutron beam with several FNRs, were designed, and the irradiation of a phantom by the neutron beam was simulated by calculations with the concentrations of ^{10}B in tumor tissue (T) and in normal tissue (N) as parameters. We calculated the advantage depth 30 (AD30), i.e., the depth in the phantom at which the tumor dose equaled 30 Gy-eq without exceeding the normal-tissue tolerance dose of 10 Gy-eq; we also calculated the irradiation time of the neutron beam that resulted in a peak normal-tissue dose of 10 Gy-eq. In the case of $T = 65$ ppm, the AD30 of the neutron beam increased when $N = 0.65$ ppm, which could be brought about by the administration of an advanced compound of boron (Miura et al., 2001), compared with that when $N = 18$ ppm, a value attainable by the use of a 4-borono-L-phenylalanine [BPA; 4-(dihydroxyboryl)-L-phenylalanine] (Kiger, et al., 2001); however, both the AD30 and the irradiation time of the neutron beam depended more strongly on the FNR value when $N = 0.65$ ppm than when $N = 18$ ppm.

Here, we extend our previous work to examine the effects of the neutron sources and moderator materials on the delivery of a therapeutic dose to deep-seated lesions, and to identify the optimal conditions for delivering sufficient doses to deep-seated lesions within short irradiation times. Our calculation model for a BSA with a Li target included a MgF_2 or CaF_2 moderator, whereas that for a BSA with a Be target included a series of Pb, Fe, and Al slabs for fast-neutron filtration in conjunction with a MgF_2 or CaF_2 moderator. The effects of the neutron sources and moderator materials on the in-phantom relative biological effectiveness (RBE) dose and the irradiation time of the neutron beam were examined with the FNR of the neutron beam as a parameter.

2. Materials and methods

As a first step, BSA models with a Li target and a MgF_2 or CaF_2 moderator that produced neutron beams with various FNR values ranging from 2×10^{-13} to 10×10^{-13} $Gy \cdot cm^2$ were designed by iterative calculations with the thickness of the moderator as a parameter by using *Monte Carlo N-Particle Transport Code* (MCNPX) (Pelowitz, 2008). The RBE dose rates for normal and tumor tissues were calculated by placing a phantom at the treatment position for each of the BSA models, and the AD30 and the irradiation time of the neutron beam were estimated. Next, we standardized the therapeutic depth of the neutron beams for specific BSA models to permit a fair comparison between the BSA with a MgF_2 moderator and a Li target and one with a CaF_2 moderator and a Be target. In other words, for a certain case where the FNR value of the neutron beam was approximately 3×10^{-13} Gy·cm^2, the thicknesses of the Pb, Fe, and Al fast-neutron filters and of the CaF_2 moderator of the BSA with a Be target were determined so that the AD30 value of the neutron beam for the BSA with a CaF_2 moderator with a Be target was almost equal to that for the BSA with a MgF_2 moderator with a Li target. Then, BSA models with a Be target and a MgF_2 or CaF_2 moderator that produced neutron beams with various FNR values were designed with the thickness of the moderator as a parameter, and the in-phantom RBE dose and the irradiation time of the neutron beam were calculated.

Figures 1 and 2 show the calculation model for the BSA with a Li target and a MgF_2 moderator that produces a neutron beam with an FNR value of 2.91×10^{-13} Gy·cm^2 and one for the BSA with a Be target and a CaF_2 moderator that produces a neutron beam with an FNR value of 3.01×10^{-13} Gy·cm^2, respectively. The BSA with a Li target and a MgF_2 moderator had a cylindrical MgF_2 slab (density 3.15 g·cm^{-3}) 60 cm in diameter and 24.8 cm in length. The BSA with a Be target and a CaF_2 moderator included a cylindrical Pb slab (density 11.35 g·cm^{-3}) 60 cm in diameter and 21 cm in length, a cylindrical Fe slab (density 7.86 g·cm^{-3}) 60 cm in diameter and 21 cm in length, a cylindrical Al slab (density 2.70 g·cm^{-3}) 60 cm in diameter and 30 cm in length, and a cylindrical CaF_2 slab (density 3.18 g·cm^{-3}) 60 cm in diameter and 31.5 cm in length. Furthermore, 60-cm-diameter Pb, Fe, and Al fast-neutron filters with thicknesses of 21, 21, and 30 cm, respectively, were used in all cases for BSA models with a MgF_2 or CaF_2 moderator and a Be target that produced neutron beams with various FNR values.

Other components of the BSA model with the Li or Be target were a 130-cm-diameter cylindrical Pb reflector for neutrons, a 130-cm-diameter, 0.2-cm-thick Cd disk (density 8.65 g·cm^{-3}) for thermal neutron absorption; a 130-cm-diameter, 6.5-cm-thick Bi disk (density 9.75 g·cm^{-3}) for high-energy photon filtration; a 130-cm-diameter, 13-cm-thick neutron shield made of a material (density 1.40 g·cm^{-3}) containing equal weight fractions of polyethylene and LiF [^{6}Li (7.4%), ^{7}Li (92.6%)] for capturing neutrons; and a 130-cm-diameter, 1-cm-thick Pb photon shield for scattering prompt γ-rays from the (n,γ) reaction in the polyethylene. The dimensions of these components were identical to those previously used in a calculation model for a BSA with a MgF_2 moderator and a Li target driven by protons of 2.8 MeV, which produces a neutron beam with an FNR of 6×10^{-13} Gy·cm^2 (Hiraga and Ooie, 2019). The collimator with a conically shaped Pb wall 5-cm-thick had an aperture with a base diameter of 46 cm and a top diameter of 12 cm, and the distance between the neutron beam port and the treatment position was set at 1 cm. To estimate the performances of the collimator, neutron shield, and photon shield, we calculated the neutron-dose rate at the collimator aperture and that on the Pb photon shield 25 cm away from the beam axis. The calculations for the BSA models with a Li or Be target showed that the ratio of the neutron dose rate on the Pb photon shield 25 cm away from the beam axis to that at the collimator aperture did not exceed 0.8 or 1.4%, respectively.

The accelerator beam power governs the irradiation time of the neutron beam, and depends on the design and neutron source of the BSA. For example, an experimental BSA with a Li target was driven by

56 kW beam of 2.8 MeV protons (Forton et al., 2009), whereas a BSA with a Be target, constructed for use in clinical trials, was driven by 30 kW beam of 30 MeV protons (Tanaka et al., 2009). However, for the sake of simplicity, we limited ourselves to the specific case that the proton-beam power for the Li target was the same as that for the Be target, i.e., the Li and Be targets were driven by 40 kW beams of 2.8 or 30 MeV protons, respectively.

In neutron sources for commercialized BSAs, a rotating disk with a large area has been used for a Li target (Neutron Therapeutics, 2016), whereas a stationary target with a smaller area than that of the Li target has been adopted for a Be target (Sumitomo Heavy Industries, Ltd., 2020). This difference in target configuration might induce differences in the neutron beams. Therefore, for the present study we assumed that the Li and Be targets (density 0.53 or 1.85 $g \cdot cm^{-3}$, respectively) were disks of identical diameter (15 cm), thereby eliminating any effect of the target geometry on the neutron beam. To reduce heating of the targets by the incident proton beams, the thicknesses of the Li and Be targets were set to 0.014 and 0.55 cm, respectively, so that the Bragg peak of the incident protons did not occur within the targets. We assumed that each target was laminated with a 0.3-cm-thick zone of H_2O to remove the heat produced by the initial protons and was installed on a 0.5-cm-thick Cu vessel. Further, we assumed that the region of the surface of each target that was uniformly irradiated by the monodirectional proton beam was a 10.6 × 10.6 cm square at the center of the target. The distance between the Cu vessel for the Li target and the MgF_2 or CaF_2 moderator was set to 1 cm, and the distance between the Cu vessel for the Be target and the Pb slab for fast-neutron filtration was set to 1 cm. Neutron generation in the Li target was not calculated in the Monte Carlo simulation. The neutron yield per kilowatt of proton-beam power (4.45×10^{11} $s^{-1} \cdot kW^{-1}$), the energy spectra, and the angular distributions of neutrons from the $^7Li(p,n)$ reaction were based on theoretical calculations (Lee and Zhou, 1999), and were used as source terms for the MCNPX. Numerical evaluations in the MCNPX for neutron production in the Be target were based on the Bertini model (Bertini, 1963), and the neutron yield per kilowatt of proton-beam power was estimated to be 4.94×10^{12} $s^{-1} \cdot kW^{-1}$.

Figure 3 shows the neutron spectra calculated for a cylindrical cell tally 15 cm in diameter and 0.1 cm in length, which was placed behind the Cu vessel for each target as drawn in Figs. 1 and 2. The neutron spectrum for the Li target includes hardly any neutrons with energies of more than 1 MeV, whereas the neutron fluxes for energies in the range 10^{-4} to 0.1 MeV for the Li target are over almost 40% of the corresponding values for the Be target.

To examine the therapeutic dose as a function of the FNR, several BSA models were designed by changing the thickness of the MgF_2 or CaF_2 moderator so that the FNR value of the neutron beam became approximately 2×10^{-13}, 3×10^{-13}, 4×10^{-13}, 5×10^{-13}, 6×10^{-13}, 7×10^{-13}, 8×10^{-13}, 9×10^{-13}, or 10×10^{-13} $Gy \cdot cm^2$. The FNR and PHR at the treatment position were then estimated from the expressions $\int_{10\mathrm{keV}}^{50\mathrm{MeV}} K_n(E)\varphi(E)dE / \int_{0.5\mathrm{eV}}^{10\mathrm{keV}} \varphi(E)dE$ and $\int_{10\mathrm{keV}}^{50\mathrm{MeV}} K_p(E)\Phi_p(E)dE / \int_{0.5\mathrm{eV}}^{10\mathrm{keV}} \varphi(E)dE$, respectively, where $\varphi(E)$ and $\Phi_p(E)$ are, respectively, the neutron and photon spectra [$cm^{-2} \cdot s^{-1} \cdot eV^{-1}$] in free air, $K_n(E)$ is the ICRU-63 neutron kerma coefficient [$Gy \cdot cm^2$] for soft tissue, and $K_p(E)$ is the ICRP-74 photon kerma coefficient [$Gy \cdot cm^2$] for air. The values of $K_p(E)$ at energies over 10 MeV were extrapolated from the corresponding values at energies below 10 MeV. With regard to the quality of the incident beam, the ratio of the thermal neutron flux to the epithermal neutron flux (TNR) and the ratio of the total neutron current to the total neutron flux (J_T/φ_T), which provides a measure of the fraction of neutrons that are moving in the forward-beam direction and might affect the depth dose of neutrons (IAEA, 2001), were also calculated. For the estimation of the J_T/φ_T, the values of the total neutron current (J_T) and total neutron flux (φ_T) were calculated by a surface tally type 1 and a surface tally type 2 (Pelowitz, 2008), respectively; these tallies were 12 cm in diameter and were placed on the neutron beam port and modified by a tally segment card. The values other than J_T/φ_T were calculated by means of a cylindrical cell tally 10 cm in diameter and 0.1 cm in length placed on the treatment position. For the neutron cross section library, we used FXJH7 (Sasa et al., 2008), which includes reaction data for neutrons with energies of more than 20 MeV. To improve the tally convergence in MCNPX calculations, we used geometry splitting and Russian roulette as a variance-reduction technique (Booth, 1985).

Simulation calculations to obtain the position-dependent neutron or photon spectra in the phantom were performed by using the thermal-neutron-scattering law of bound hydrogen in a water molecule (Nelkin, 1960) for a cylindrical phantom 18.6 cm in diameter and 24 cm in length placed at the treatment positions of the BSA model. The cylindrical phantom (density 1.03 $g \cdot cm^{-3}$) had the chemical composition specified in *ICRP-1975* and contained ^{10}B atoms at a concentration of 0.65 ppm for an advanced compound or 18 ppm for BPA. Calculations of the in-phantom spectra included the normal-tissue ^{10}B concentration to incorporate the effects of neutron absorption by ^{10}B and the resultant prompt 477-keV photons on the position-dependent neutron and photon spectra. The position-dependent neutron or photon spectra along the axis of the phantom were calculated by using a mesh tally 16 cm in length consisting of 201 cells in a rectangular parallelepiped array of $0.0796 \times 2 \times 2$ cm.

The ^{10}B concentrations in tumor (T) and normal tissue (N) were assumed to be 65 and 18 ppm, respectively, for BPA, and 65 and 0.65ppm, respectively, for an advanced compound. The boron dose rate was obtained by multiplying the neutron spectrum by the kerma coefficient for the $^{10}B(n,\alpha)$ reaction [in units of $Gy \cdot cm^2 \cdot (\mu g\ ^{10}B)^{-1}$] (Yonai et al., 2003) and then integrating over the neutron energy. The neutron-dose rate was obtained by multiplying the neutron spectrum by the Dosimetry System 2002 (DS_{02}) neutron kerma coefficient for soft tissue (Egbert, 2012) and integrating over the neutron energy. The photon dose rate was similarly obtained by multiplying the photon spectrum by the DS_{02} photon kerma coefficient for soft tissue (Egbert, 2012) and integrating over the photon energy. The number of histories to be run in the problem was 2×10^9. As for the in-phantom dose rate calculations, the relative errors of the mesh tally corresponding to one standard deviation for the BSAs with a Be target and a MgF_2 or CaF_2 moderator were greater than those for the BSAs with a Li target and a MgF_2 of CaF_2 moderator; however, the relative errors of a mesh tally at a 10 cm depth in a phantom for the neutron dose rate, boron dose rate, and photon dose rate did not exceed 2.6, 0.4, and 2.6 %, respectively.

The tumor and normal-tissue RBE dose rates were calculated from the sum of the boron, neutron, and photon dose rates with compound factors for the tumor and normal tissue of 3.8 and 1.3, respectively, and with RBE values of 3.2 for neutrons and 1.0 for photons (Bleuel et al., 1998). The irradiation time of the neutron beam was estimated from the ratio of 10 Gy-eq to the peak of the normal-tissue RBE dose rate. The tumor RBE dose was then calculated by multiplying the tumor RBE dose rate by the irradiation time. The following figures of merit were estimated from the tumor RBE dose profiles along the phantom axis: the advantage depth (AD; the depth in the phantom where the tumor RBE dose is equal to 10 Gy-eq), the advantage depth 30 (AD30; the depth in the phantom where the tumor RBE dose is equal to 30 Gy-eq), and the advantage ratio (AR; the ratio of the integral tumor RBE dose to the normal-tissue RBE dose averaged from the neutron beam entrance to the advantage depth).

Clinical trials of BNCT have shown that a median survival time of 13 months for patients with glioblastoma multiforme was achieved by administration of tumor doses in the range 18 to 55 Gy-eq (Chanana et al., 1999). The treatment efficacy for deep-seated tumors is therefore dominated by the AD30 rather than the AD, and the AD30 can be considered as an indicator of therapeutic depth. Furthermore, the clinical acceptability of AB-BNCT would be increased by reducing the irradiation time of the neutron beam, because a short irradiation time would reduce the time for which a patient would need to be immobilized.

3. Results and discussion

3.1. Effects of neutron sources and moderator materials on BSA characteristics and irradiation times as a function of FNR

The dependence on the FNR of the thickness of the MgF_2 or CaF_2 moderator ($T_{\mathrm{Li\_MgF_2}}$, $T_{\mathrm{Li\_CaF_2}}$, $T_{\mathrm{Be\_MgF_2}}$, $T_{\mathrm{Be\_CaF_2}}$); the values of PHR, TNR, and J_T/φ_T, the fluxes of epithermal neutrons at the treatment position ($\varphi_{\mathrm{Li\_MgF_2}}$, $\varphi_{\mathrm{Li\_CaF_2}}$, $\varphi_{\mathrm{Be\_MgF_2}}$, $\varphi_{\mathrm{Be\_CaF_2}}$); and the irradiation times for the normal-tissue ^{10}B concentrations (N) of 0.65 and 18 ppm ($IT_{\mathrm{Li\_MgF_2}}$, $IT_{\mathrm{Li\_CaF_2}}$, $IT_{\mathrm{Be\_MgF_2}}$, $IT_{\mathrm{Be\_CaF_2}}$) are summarized in Tables 1–4, for the MgF_2 moderator with the Li target, the CaF_2 moderator with the Li target, the MgF_2 moderator with the Be target, and the CaF_2 moderator with the Be target, respectively.

In Tables 1–4, the epithermal neutron fluxes increase with increasing FNR because the thickness of the moderator decreases with increasing FNR. Each of the PHR and TNR values meets the target number of 2×10^{-13} Gy·cm^2 and 5%, respectively, as given in *IAEA TECDOC-1223* (IAEA, 2001). Changes in the PHRs and TNRs due to an increase in FNR should hardly affect the in-phantom photon dose rate and the in-phantom neutron-dose rate, respectively, because each of the PHR and TNR values is rather small. The PHRs decrease with increasing FNR because the numbers of epithermal neutron fluxes increase with increasing FNR. None of the J_T/φ_T values reaches the target number of 0.7 given in *IAEA TECDOC-1223* (IAEA, 2001) because the length of the collimator (14 cm) is rather short. The irradiation times for N =0.65 or 18 ppm decrease with increasing the FNR because the peak of the in-phantom neutron-dose rate and the resultant peak of the normal-tissue RBE dose rate increase with increasing epithermal neutron flux. Furthermore, a comparison of numbers in the same row of the tables shows that the irradiation times for N = 0.65 ppm are longer than those for N = 18 ppm; This is because the in-phantom boron dose rate and the resultant peak of the normal-tissue RBE dose rate for N = 0.65 ppm are smaller than those for N = 18 ppm.

In the case of the Li target, a comparison of numbers in the same row of Tables 1 and 2 shows that the thicknesses of MgF_2 moderators are smaller than those of CaF_2 moderators that have almost the same FNRs as the MgF_2 moderators, i.e. $T_{\mathrm{Li\_MgF_2}}(\mathrm{FNR}) < T_{\mathrm{Li\_CaF_2}}(\mathrm{FNR})$. This might be related to the fact that the epithermal neutron fluxes for the MgF_2 moderators are greater than those of the CaF_2 moderators, i.e., $\varphi_{\mathrm{Li\_MgF_2}}(\mathrm{FNR}) > \varphi_{\mathrm{Li\_CaF_2}}(\mathrm{FNR})$. Furthermore, the irradiation times are approximately inversely proportional to the epithermal neutron fluxes, because the peak of the normal-tissue RBE dose rate is approximately proportional to the epithermal neutron flux. In other words, the relationship $IT_{\mathrm{Li\_MgF_2}}(\mathrm{FNR})/IT_{\mathrm{Li\_CaF_2}}(\mathrm{FNR}) \approx \varphi_{\mathrm{Li\_CaF_2}}(\mathrm{FNR})/\varphi_{\mathrm{Li\_MgF_2}}(\mathrm{FNR})$ holds. The irradiation times for the MgF_2 moderators are, therefore, shorter than those for the CaF_2 moderators, i.e., $IT_{\mathrm{Li\_MgF_2}}(\mathrm{FNR}) < IT_{\mathrm{Li\_CaF_2}}(\mathrm{FNR})$ for N = 0.65 and 18 ppm, respectively, because the relationship $\varphi_{\mathrm{Li\_CaF_2}}(\mathrm{FNR})/\varphi_{\mathrm{Li\_MgF_2}}(\mathrm{FNR}) < 1$ holds. These arguments are also valid in the case of the Be target, i.e., $T_{\mathrm{Be\_MgF_2}}(\mathrm{FNR}) < T_{\mathrm{Be\_CaF_2}}(\mathrm{FNR})$; $\varphi_{\mathrm{Be\_MgF_2}}(\mathrm{FNR}) > \varphi_{\mathrm{Be\_CaF_2}}(\mathrm{FNR})$; $IT_{\mathrm{Be\_MgF_2}}(\mathrm{FNR}) < IT_{\mathrm{Be\_CaF_2}}(\mathrm{FNR})$ for N = 0.65 and 18 ppm, respectively, as can be confirmed by comparing Tables 3 and 4.

In the case of the CaF_2 moderators, comparing numbers in the same row of Tables 2 and 4 shows that the epithermal neutron fluxes for the CaF_2 moderators with the Be target are greater than those of the CaF_2 moderators with the Li target, i.e., $\varphi_{\mathrm{Be\_CaF_2}}(\mathrm{FNR}) > \varphi_{\mathrm{Li\_CaF_2}}(\mathrm{FNR})$; Moreover, the irradiation times for the CaF_2 moderators with the Be target are shorter than those of the CaF_2 moderators with the Li target, i.e., $IT_{\mathrm{Be\_CaF_2}}(\mathrm{FNR}) < IT_{\mathrm{Li\_CaF_2}}(\mathrm{FNR})$ for N = 0.65 and 18 ppm, respectively. This is because the neutron-generation rate of 4.94×10^{12} $s^{-1} \cdot kW^{-1}$ for the Be target is greater than that of 4.45×10^{11} $s^{-1} \cdot kW^{-1}$ for the Li target. These arguments are also valid for the MgF_2 moderators, i.e., $\varphi_{\mathrm{Be\_MgF_2}}(\mathrm{FNR}) > \varphi_{\mathrm{Li\_MgF_2}}(\mathrm{FNR})$; $IT_{\mathrm{Be\_MgF_2}}(\mathrm{FNR}) < IT_{\mathrm{Li\_MgF_2}}(\mathrm{FNR})$ for N = 0.65 and 18 ppm, respectively, as can be confirmed by comparing Tables 1 and 3. However, there are exceptions, i.e., $\varphi_{\mathrm{Be\_MgF_2}}(1.94 \times 10^{-13}) < \varphi_{\mathrm{Li\_MgF_2}}(2.05 \times 10^{-13})$; $IT_{\mathrm{Be\_MgF_2}}(1.94 \times 10^{-13}) > IT_{\mathrm{Li\_MgF_2}}(2.05 \times 10^{-13})$ for N = 0.65 and 18 ppm, respectively. These exceptions might occur because the total thickness of the Pb, Fe, and Al slabs for fast-neutron filtration and the MgF_2 moderator of 99.1 cm for an FNR of 1.94×10^{-13} $Gy \cdot cm^2$ for the Be target is markedly greater than the thickness of 27.2 cm for a MgF_2 moderator for an FNR of 2.05×10^{-13} $Gy \cdot cm^2$ for the Li target.

3.2. Effects of neutron sources and moderator materials on the in-phantom tumor RBE dose as a function of FNR

Figures 4 and 5 show the dependence on the FNR of the AD30 of the neutron beam for BSA models with a Li or Be target and a MgF_2 or CaF_2 moderator (denoted henceforth as Li_MgF_2, Li_CaF_2, Be_MgF_2, and Be_CaF_2, respectively) and when T/N = 100 (T = 65 ppm, N = 0.65 ppm) or T/N = 3.61 (T = 65 ppm, N = 18 ppm). Figure 4 shows that when T/N = 100, the AD30 values for Li_MgF_2 are almost identical to those for Li_CaF_2, which have almost the same FNRs as Li_MgF_2. This is also seen in Fig. 5 when T/N = 3.61. For the Li target, the MgF_2 moderator is superior to the CaF_2 moderator, because the irradiation times for N = 0.65 ppm or 18 ppm for the MgF_2 moderators are shorter than those for the CaF_2 moderators, which have almost the same FNRs as the MgF_2 moderators, as detailed in Tables 1 and 2.

Figure 4 shows that when $T/N = 100$, the AD30 of the neutron beam with an FNR of 2.05×10^{-13} Gy·cm^2 for Li_MgF$_2$ is 1 cm longer than that for an FNR of 9.96×10^{-13} Gy·cm^2 for Li_MgF$_2$. Figure 5 shows that when $T/N = 3.61$, the AD30 of the neutron beam with an FNR of 2.05×10^{-13} Gy·cm^2 for Li_MgF$_2$ is 0.1 cm shorter than that for an FNR of 9.96×10^{-13} Gy·cm^2 for Li_MgF$_2$. These changes in the AD30 on changing the FNR almost agree with those found in our previous study (Hiraga and Ooie, 2019), in which the AD30 values of the neutron beam were calculated for a BSA model that included a MgF_2 moderator and a Li target driven by protons of 2.8 MeV. Figure 4 shows that when $T/N = 100$, there are some cases that the AD30 values for Be_MgF$_2$ are smaller than the corresponding values for Be_CaF$_2$. This is also seen in Fig. 5, when $T/N = 3.61$. The differences in the AD30 values of Be_MgF$_2$ and Be_CaF$_2$ are not brought about by differences in the J_T/φ_T values of the neutron beam, because each of these values for the MgF_2 moderator with the Be target is almost identical to the corresponding value for the CaF_2 moderator with the Be target, as detailed in Tables 3 and 4.

Figure 4 shows that when $T/N = 100$, the AD30 values for Li_MgF$_2$, Li_CaF$_2$, Be_MgF$_2$, and Be_CaF$_2$ vary greatly depending on the FNR, and peak at an FNR of about 3×10^{-13} Gy·cm^2. Figure 5 shows that when $T/N = 3.61$, the AD30 values for Li_MgF$_2$, Li_CaF$_2$, Be_MgF$_2$, and Be_CaF$_2$ change slightly depending on the FNR, and are smaller than the corresponding values for $T/N = 100$, and are almost saturated at an FNR of about 10×10^{-13} Gy·cm^2. These results show that a neutron beam with an FNR value of about 3×10^{-13} or 10×10^{-13} Gy·cm^2 is an optimal choice for the delivery of therapeutic doses to deep-seated lesions when $T/N = 100$ or 3.61, respectively. Further, these results suggest that stricter control over FNR is required when T/N ratio increases. Figure 4 shows that when $T/N = 100$, the AD30 value of the neutron beam with an FNR of 3.01×10^{-13} Gy·cm^2 for Be_CaF$_2$ is almost identical to that for an FNR of 2.91×10^{-13} Gy·cm^2 for Li_MgF$_2$. This is also seen in Fig. 5, when $T/N = 3.61$.

Because BPA has been widely applied to BNCT, close attention should be paid to the case of $T/N = 3.61$. Figure 5 shows that when $T/N = 3.61$, the AD30 value of the neutron beam with an FNR of 10.06×10^{-13} Gy·cm^2 for the Be_MgF$_2$ is almost identical to that for the neutron beam with an FNR of 10.05×10^{-13} Gy·cm^2 for the Be_CaF$_2$, and slightly greater than those for the neutron beams with the FNR of about 10×10^{-13} Gy·cm^2 for Li_MgF$_2$ and Li_CaF$_2$. Moreover, the irradiation time for $N = 18$ ppm of the neutron beam with an FNR of 10.06×10^{-13} Gy·cm^2 for Be_MgF$_2$ was 80.7 s shorter than that for the neutron beam with an FNR of 10.05×10^{-13} Gy·cm^2 for Be_CaF$_2$, as detailed in Tables 3 and 4. We therefore conclude that a BSA with a Be target and a MgF_2 moderator that produces the neutron beam with an FNR value of about 10×10^{-13} Gy·cm^2 is the optimal choice for the delivery of sufficient doses to deep-seated lesions in short irradiation times when BPA is adopted as a boron carrier.

Figures 6 and 7 show the dependence on the FNR of the AD of the neutron beam for BSA models with a Li or Be target with a MgF_2 or CaF_2 moderator when $T/N = 100$ ($T = 65$ ppm, $N = 0.65$ ppm) or $T/N = 3.61$ ($T = 65$ ppm, $N = 18$ ppm). The dependence on the FNR of the AD is similar to the dependence on the FNR of the AD30. When $T/N = 3.61$, the AD value of the neutron beam with an FNR of 10.06×10^{-13} Gy·cm^2 for the Be_MgF$_2$ is almost identical to that for the neutron beam with an FNR of 10.05×10^{-13} Gy·cm^2 for the Be_CaF$_2$, and slightly greater than those for the neutron beams with the FNR of about

10×10^{-13} Gy·cm^2 for Li_MgF$_2$ and Li_CaF$_2$. In consideration of the advantage that the irradiation time for $N = 18$ ppm for a neutron beam with an FNR of 10.06×10^{-13} Gy·cm^2 for Be_MgF$_2$ is shorter than that for a neutron beam with an FNR of 10.05×10^{-13} Gy·cm^2 for Be_CaF$_2$, a BSA with a Be target and a MgF_2 moderator that produces a neutron beam with an FNR value of about 10×10^{-13} Gy·cm^2 is again suitable to realize sufficient AD values within short irradiation times when BPA is adopted as a boron carrier.

Figures 8 and 9 show the dependence on the FNR of the AR of the neutron beam for BSA models with a Li or Be target and a MgF_2 or CaF_2 moderator when $T/N = 100$ ($T = 65$ ppm, $N = 0.65$ ppm) or $T/N = 3.61$ ($T = 65$ ppm, $N = 18$ ppm). Figure 8 shows that when $T/N = 100$, each of the AR values for Li_MgF$_2$, Li_CaF$_2$, Be_MgF$_2$, and Be_CaF$_2$ decreases almost linearly as the FNR is increased to 10×10^{-13} Gy·cm^2. This is also seen in Fig. 9, when $T/N = 3.61$. These changes in the AR as a result of changes in the FNR agree with the known property that AR values generally decrease on increasing the rate of fast neutrons in a neutron beam (Binns et al., 2005). To upgrade the dosimetric specificity and selectivity in BNCT, a high value of AR of the neutron beam is desired. In consideration of this fact, it is undesirable to use neutron beams with too high values of FNR. We therefore think that it was appropriate to set the upper limit of FNR to about 10×10^{-13} Gy·cm^2.

4. Conclusions

We assumed that the Li and Be targets were driven by 40-kW beams of 2.8 or 30 MeV protons, respectively and that the configuration of the Li target was the same as that of the Be target. BSA models with a Li or Be target and a MgF_2 or CaF_2 moderator that produced neutron beams with various FNR values ranging from 2×10^{-13} to 10×10^{-13} Gy·cm^2 were designed by iterative calculations with the thickness of the moderator as a parameter; the AD30, AD, AR, and irradiation time of the neutron beam for the BSAs were then examined with the FNR of the neutron beam as a parameter. Fast-neutron filters for the BSA models with a Be target were designed so that the AD30 value of the neutron beam for the BSA with a CaF_2 moderator with a Be target would be almost equal to that for the BSA with a MgF_2 moderator with a Li target when the FNR of the neutron beam was approximately 3×10^{-13} Gy·cm^2. The AD30 values for Li_MgF$_2$, Li_CaF$_2$, Be_MgF$_2$, and Be_CaF$_2$ for $T/N = 100$ peaked at an FNR of about 3×10^{-13} Gy·cm^2, whereas those for $T/N = 3.61$ were almost saturated at an FNR of about 10×10^{-13} Gy·cm^2. These results showed that a neutron beam with an FNR value of about 3×10^{-13} or 10×10^{-13} Gy·cm^2 is an optimal choice for the delivery of therapeutic doses to deep-seated lesions when $T/N = 100$ or 3.61, respectively. The AR values for Li_MgF$_2$, Li_CaF$_2$, Be_MgF$_2$, and Be_CaF$_2$ for $T/N = 100$ or 3.61 decreased almost linearly as the FNR was increased to 10×10^{-13} Gy·cm^2. To upgrade the dosimetric specificity and selectivity in BNCT, a high value of AR of the neutron beam is desired. We therefore think that it was appropriate to set the upper limit of FNR to about 10×10^{-13} Gy·cm^2.

When $T/N = 100$, the AD30 values for Li_MgF$_2$, Li_CaF$_2$, Be_MgF$_2$, and Be_CaF$_2$ vary greatly depending on the FNR, and are greater than the corresponding values for $T/N = 3.61$. We therefore think that stricter control over FNR is required when T/N ratio increases. When $T/N = 3.61$, the AD30 value of the neutron beam with an FNR of 10.06×10^{-13} Gy·cm^2 for the Be_MgF$_2$ was almost identical to that for the neutron beam with an FNR of 10.05 × 10^{-13} Gy·cm^2 for the Be_CaF_2, and slightly greater than those for the neutron beams with the FNR of about 10 × 10^{-13} Gy·cm^2 for Li_MgF_2 and Li_CaF_2. Moreover, the irradiation time for N = 18 ppm of the neutron beam with an FNR of 10.06 × 10^{-13} Gy·cm^2 for Be_MgF_2 was 80.7 s shorter than that for the neutron beam with an FNR of 10.05 × 10^{-13} Gy·cm^2 for Be_CaF_2. We therefore conclude that a BSA with a Be target and a MgF_2 moderator that produces the neutron beam with an FNR value of about 10 × 10^{-13} Gy·cm^2 is the optimal choice for the delivery of sufficient doses to deep-seated lesions in short irradiation times when BPA is adopted as a boron carrier.

Acknowledgements

This work was supported by JSPS KAKENHI Grant Number JP20K05378.

References

Aihara, T., et al., 2006. First clinical case of boron neutron capture therapy for head and neck malignancies using ^{18}F–BPA PET. Head Neck 28, 850–855. https://doi.org/10.1002/hed.20418.

Bertini, H.W., 1963. Low-energy intranuclear cascade calculation. Phys. Rev. 131, 1801–1821. https://doi.org/10.1103/PhysRev.131.1801.

Binns. P.J., et al., 2005. Epithermal neutron beams for clinical studies of boron neutron capture therapy: A dosimetric comparison of seven beams. Radiat. Res. 164, 212–220. https://doi.org/10.1667/rr3404.

Bleuel, D.L., et al., 1998. Designing accelerator-based epithermal neutron beams for boron neutron capture therapy. Med. Phys. 25, 1725–1734. https://doi.org/10.1118/1.598353.

Booth, E.B., 1985. *A Sample Problem for Variance Reduction in MCNP. LA-10363-MS.* Los Alamos National Laboratory, Los Alamos, NM. https://mcnp.lanl.gov/pdf_files/la-10363.pdf.

Chanana, A.D., et al., 1999. Boron neutron capture therapy for glioblastoma multiforme: Interim results from the phase I/II dose-escalation studies. Neurosurgery 44, 1182–1192. https://doi.org/10.1097/00006123-199906000-00013.

Egbert, S.D., 2012. The 2002 dosimetry system (DS_{02}) and available fluences for organ dose calculations. Radiat. Prot. Dosimetry 149, 21–27. https://doi.org/10.1093/rpd/ncr297.

Forton, E., et al., 2009. Overview of the IBA accelerator-based BNCT system. Appl. Radiat. Isot. 67, S262–S265. https://doi.org/10.1016/j.apradiso.2009.03.099.

Fukuda, H., et al., 2003. Boron neutron capture therapy (BNCT) for malignant melanoma with special reference to absorbed doses to the normal skin and tumor. Australasian Phys. Eng. Sci. Med. 26, 97. https://doi.org/10.1007/BF03178777.

González, S.J., et al., 2004. First BNCT treatment of a skin melanoma in Argentina: Dosimetric analysis and clinical outcome. Appl. Radiat. Isot. 61, 1101–1105. https://doi.org/10.1016/j.apradiso.2004.05.060.

Hiraga, F., Ooie, T., 2019. Synergistic effects of fast-neutron dose per epithermal neutron and ^{10}B concentration on relative-biological-effectiveness dose for accelerator-based boron neutron capture therapy. Appl. Radiat. Isot. 144, 1–4. https://doi.org/10.1016/j.apradiso.2018.11.003.

IAEA, 2001. Current Status of Neutron Capture Therapy. IAEA TECDOC-1223, International Atomic

Energy Agency, Vienna. https://www-pub.iaea.org/MTCD/publications/PDF/te_1223_prn.pdf.
Kankaanranta, L., et al., 2007. Boron neutron capture therapy in the treatment of locally recurred head and neck cancer. Int. J. Radiat. Oncol. Biol. Phys. 69, 475–82. https://doi.org/10.1016/j.ijrobp.2007.03.039.
Kato, I., et al., 2004. Effectiveness of BNCT for recurrent head and neck malignancies. Appl. Radiat. Isot. 61, 1069–1073. https://doi.org/10.1016/j.apradiso.2004.05.059.
Kiger, W.S., III, et al., 2001. A pharmacokinetic model for the concentration of ^{10}B in blood after boronphenylalanine–fructose administration in humans. Radiat. Res. 155, 611–618. https://doi.org/10.1667/0033-7587(2001)155[0611:apmftc]2.0.co;2.
Kreiner, A.J., 2012. Accelerator-based BNCT, in: Sauerwein W.A.G., Wittig A., Moss R., Nakagawa Y. (Eds.), Neutron Capture Therapy: Principles and Applications. Springer: Berlin, pp. 41–54.
Lavelle, C.M., et al., 2008. Neutronic design and measured performance of the low energy neutron source (LENS) target moderator reflector assembly. Nucl. Instrum. Methods Phys. Res., Sect. A 587, 324–341. https://doi.org/10.1016/j.nima.2007.12.044
Lee, C.L., Zhou, X.-L., 1999. Thick target neutron yields for the $^{7}Li(p,n)^{7}Be$ reaction near threshold. Nucl. Instrum. Methods Phys. Res., Sect. B 152: 1–11. https://doi.org/10.1016/S0168-583X(99)00026-9.
Montagnini, B., et al., 2002. Spectrum shaping of accelerator-based neutron beams for BNCT. Nucl. Instrum. Methods Phys. Res., Sect. A 476, 90–98. https://doi.org/10.1016/S0168-9002(01)01398-5.
Miura, M., et al., 2001. Boron neutron capture therapy of a murine mammary carcinoma using a lipophilic carboranyltetraporphyrin. Radiat. Res. 155, 603–610. https://doi.org/10.1667/0033-7587(2001)155[0603:BNCTOA]2.0.CO;2.
Nava, E., Rosi, G., 2009. BNCT at the TAPIRO Reactor, in: Sauerwein W.A.G., Moss R.L. (Eds.) Requirements for Boron Neutron Capture Therapy (BNCT) at a Nuclear Research Reactor, EUR 23830, European Commission Joint Research Centre Institute for Energy, Petten, The Netherlands, Chap. 6.13, pp. 116–119. https://op.europa.eu/en/publication-detail/-/publication/f4179a3b-ae37-46f8-9820-f0857d85c5fa/language-en (accessed 16 June 2022).
Nelkin, M., 1960. Scattering of slow neutrons by water. Phys. Rev. 119, 741–746. https://doi.org/10.1103/PhysRev.119.741.
Neutron Therapeutics, 2016. https://www.neutrontherapeutics.com/technology/ (accessed 15 June 2020).
Pelowitz, D.B., 2008. MCNPX User's Manual Version 2.6.0. LA-CP-07-1473. https://www.mcnp.ir/admin/imgs/1354176297.2.6.0_Users_Manual.pdf (accessed 15 July 2019).
Sasa, T., et al., 2008. Continuous Energy Cross Section Library for MCNP/MCNPX Based on JENDL High Energy File 2007; FXJH7. JAEA-Data/Code 2008-022, Japan Atomic Energy Agency, Tōkai, Japan. https://jopss.jaea.go.jp/pdfdata/JAEA-Data-Code-2008-022.pdf (accessed on 15 June 2022).
Speziale, S., Duffy, T., 2002. Single-crystal elastic constants of fluorite (CaF_2) to 9.3 GPa. Phys. Chem. Miner. 29, 465-472. https://doi.org/10.1007/s00269-002-0250-x.
Sumitomo Heavy Industries, Ltd., 2020. https://www.shi.co.jp/english/info/2019/6kgpsq0000002ji0.html (accessed 15 June 2022).
Tahara, Y., et al., 2006. Engineering design of a spallation reaction-based neutron generator for boron

neutron capture therapy. J. Nucl. Sci. Technol. 43, 9–19. https://doi.org/10.1080/18811248.2006.9711063.
Tanaka, H., et al., 2009. Characteristics comparison between a cyclotron-based neutron source and KUR-HWNIF for boron neutron capture therapy. Nucl. Instrum. Methods Phys. Res., Sect. B 267, 1970–1977. https://doi.org/10.1016/j.nimb.2009.03.095.
Torres-Sánchez, P., et al., 2021. Optimized beam shaping assembly for a 2.1-MeV proton-accelerator-based neutron source for boron neutron capture therapy. Sci. Rep. 11, 7576. https://doi.org/10.1038/s41598-021-87305-9.
Yonai, S., et al., 2003. Feasibility study on epithermal neutron field for cyclotron-based boron neutron capture therapy. Med. Phys. 30, 2021–2030. https://doi.org/10.1118/1.1587431.

Figure captions

Fig. 1. Axial section of a BSA model with a Li target and a MgF_2 moderator that produces a neutron beam with an FNR value of 2.91×10^{-13} Gy·cm^2

Fig. 2. Axial section of a BSA model with a Be target and a CaF_2 moderator that produces a neutron beam with an FNR value of 3.01×10^{-13} Gy·cm^2

Fig. 3. Neutron spectra in free air in the region behind the Cu vessel for the Li or Be target

Fig. 4. Dependence on the FNR of the AD30 of the neutron beam for BSA models with a Li or Be target and a MgF_2 or CaF_2 moderator when $T/N = 100$ ($T = 65$ ppm, $N = 0.65$ ppm)

Fig. 5. Dependence on the FNR of the AD30 of the neutron beam for BSA models with a Li or Be target and a MgF_2 or CaF_2 moderator when $T/N = 3.61$ ($T = 65$ ppm, $N = 18$ ppm)

Fig. 6. Dependence on the FNR of the AD of the neutron beam for BSA models with a Li or Be target and a MgF_2 or CaF_2 moderator when $T/N = 100$ ($T = 65$ ppm, $N = 0.65$ ppm)

Fig. 7. Dependence on the FNR of the AD of the neutron beam for BSA models with a Li or Be target and a MgF_2 or CaF_2 moderator when $T/N = 3.61$ ($T = 65$ ppm, $N = 18$ ppm)

Fig. 8. Dependence on the FNR of the AR of the neutron beam for BSA models with a Li or Be target and a MgF_2 or CaF_2 moderator when $T/N = 100$ ($T = 65$ ppm, $N = 0.65$ ppm)

Fig. 9. Dependence on the FNR of the AR of the neutron beam for BSA models with a Li or Be target and a MgF_2 or CaF_2 moderator when $T/N = 3.61$ ($T = 65$ ppm, $N = 18$ ppm)

Tables

Table 1. Dependence of BSA characteristics and irradiation times (*IT*) on the FNR for a MgF_2 moderator and a Li target

Table 2. Dependence of BSA characteristics and irradiation times on the FNR for a CaF_2 moderator and a Li target

Table 3. Dependence of BSA characteristics and irradiation times on the FNR for a MgF_2 moderator and a Be target

Table 4. Dependence of BSA characteristics and irradiation times on FNR for a CaF_2 moderator and a Be target

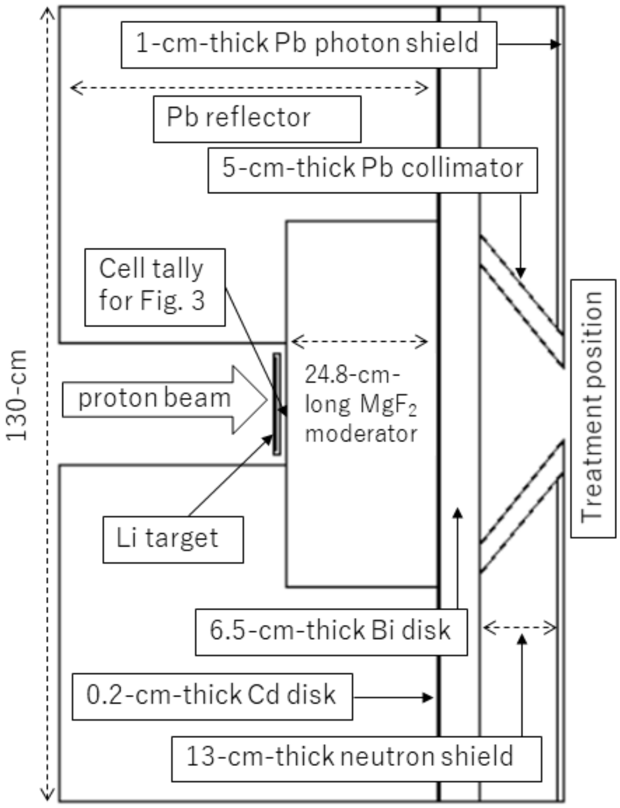

Fig. 1. Axial section of a BSA model with a Li target and a MgF_2 moderator that produces a neutron beam with an FNR value of 2.91×10^{-13} Gy·cm^2

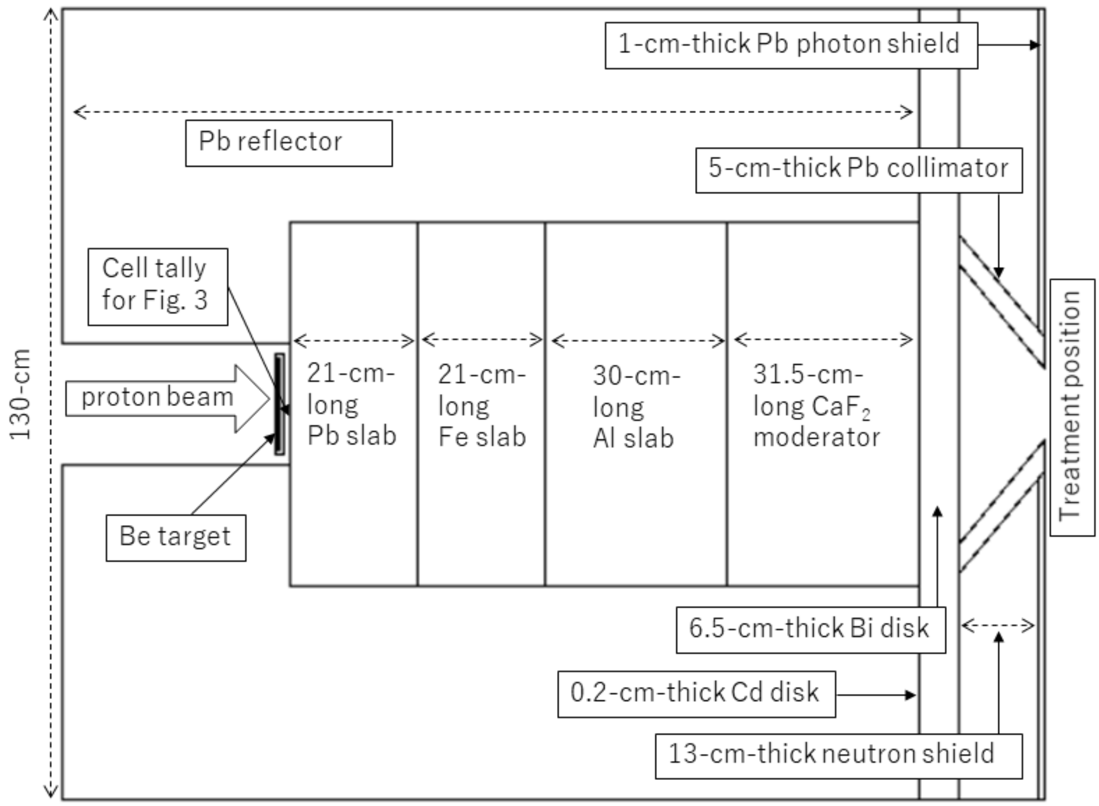

Fig. 2. Axial section of a BSA model with a Be target and a CaF_2 moderator that produces a neutron beam with an FNR value of 3.01×10^{-13} Gy·cm^2

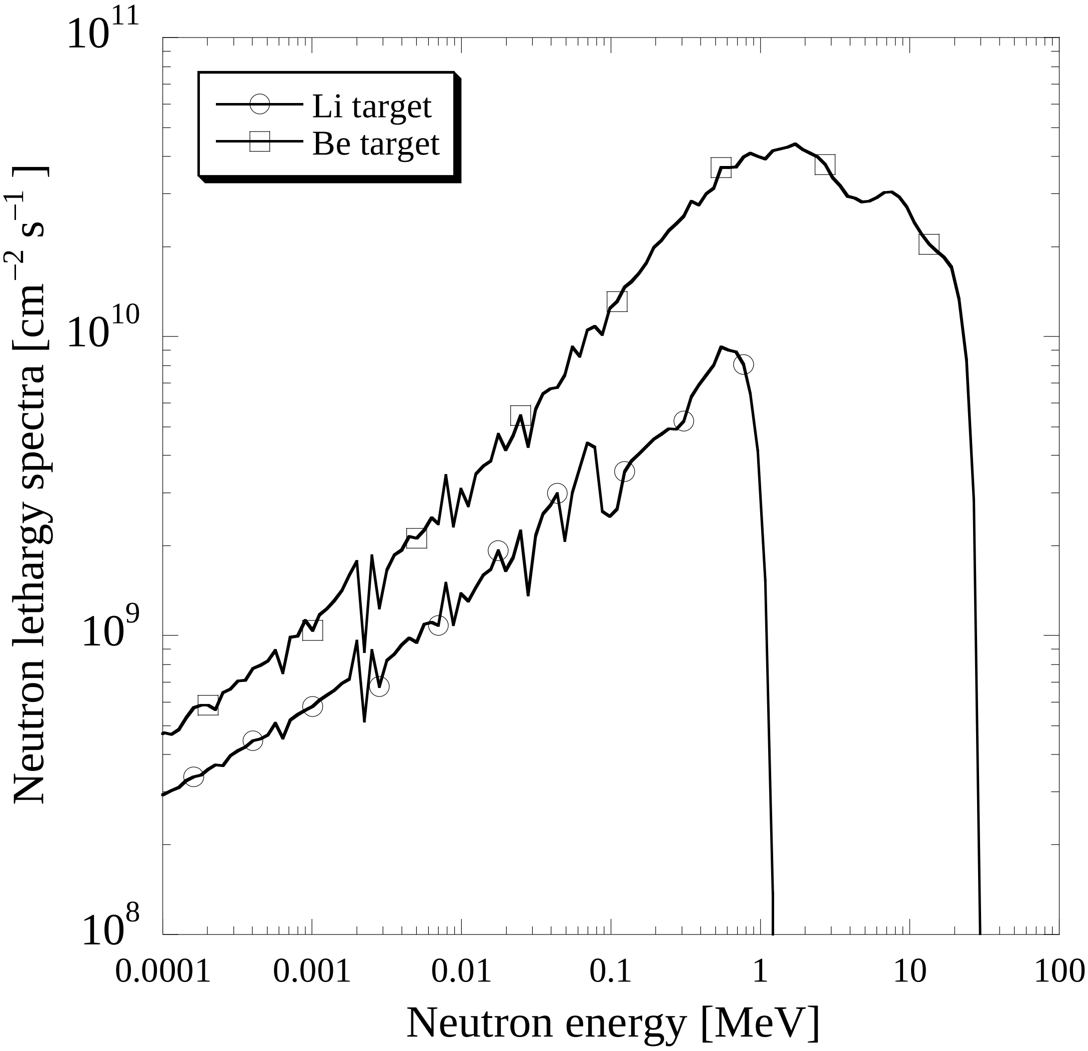

Fig. 3. Neutron spectra in free air in the region behind the Cu vessel for the Li or Be target

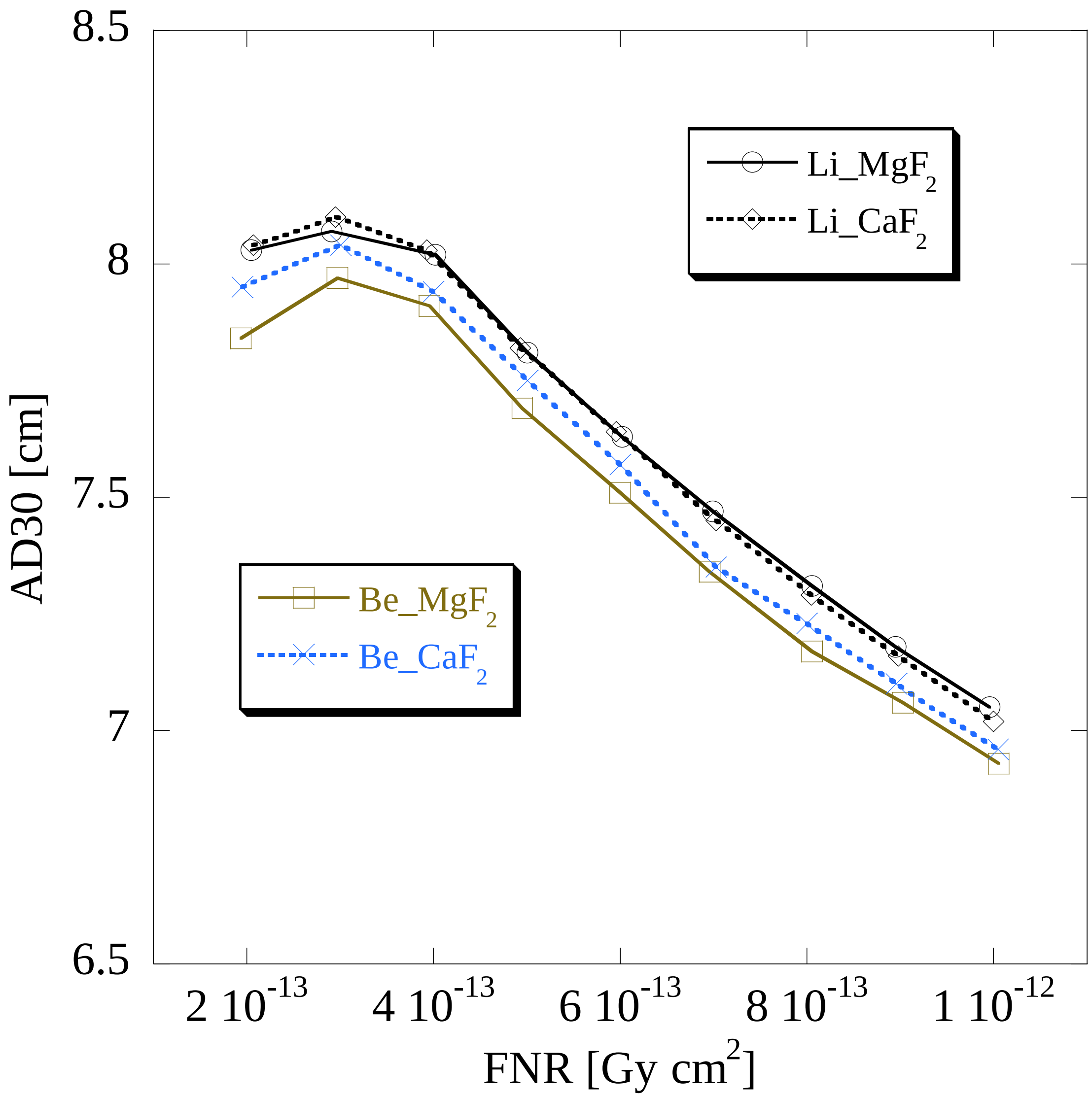

Fig. 4. Dependence on the FNR of the AD30 of the neutron beam for BSA models with a Li or Be target and a MgF_2 or CaF_2 moderator when *T*/*N* = 100 (*T* = 65 ppm, *N* = 0.65 ppm)

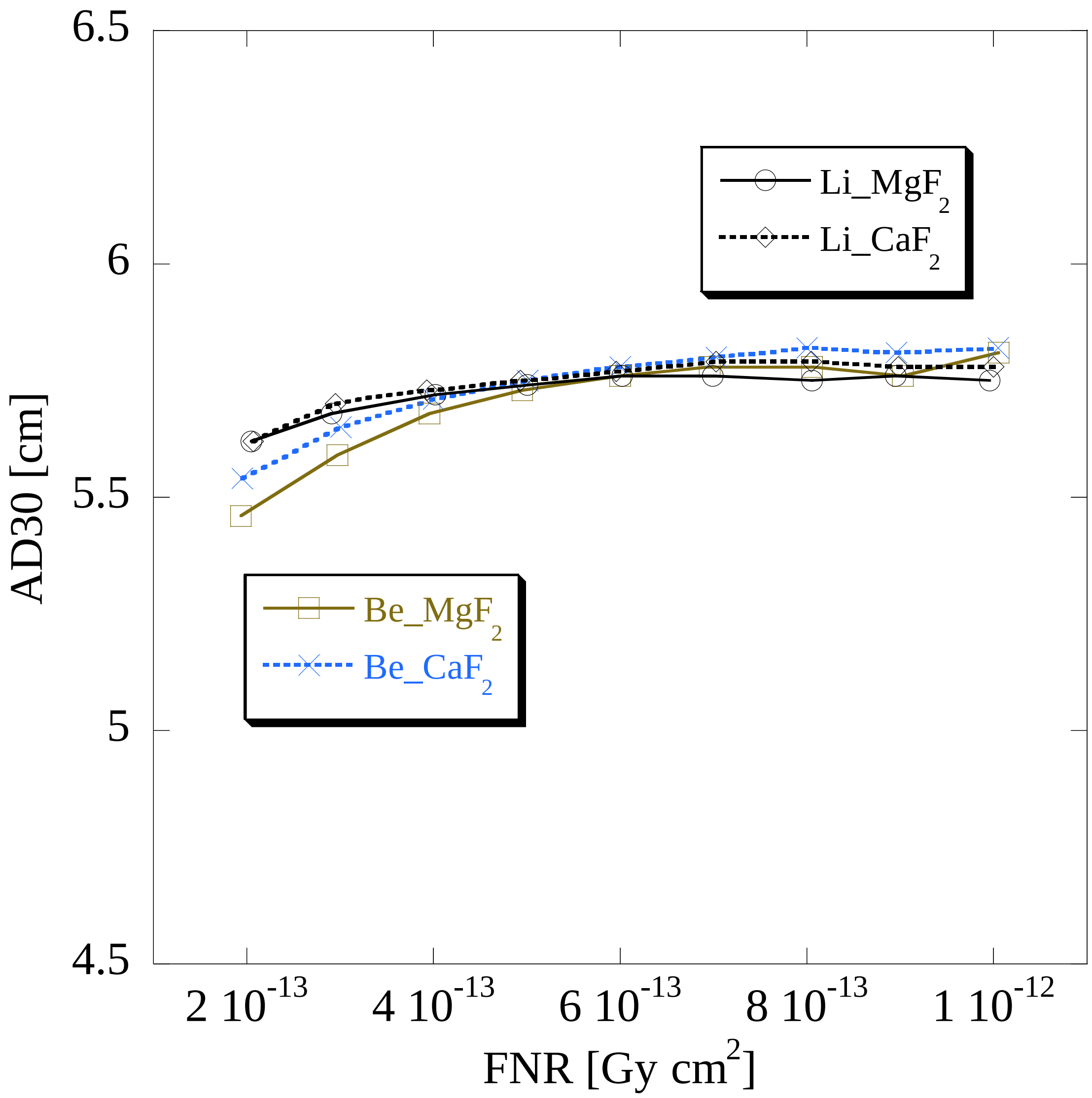

Fig. 5. Dependence on the FNR of the AD30 of the neutron beam for BSA models with a Li or Be target and a MgF_2 or CaF_2 moderator when $T/N = 3.61$ ($T = 65$ ppm, $N = 18$ ppm)

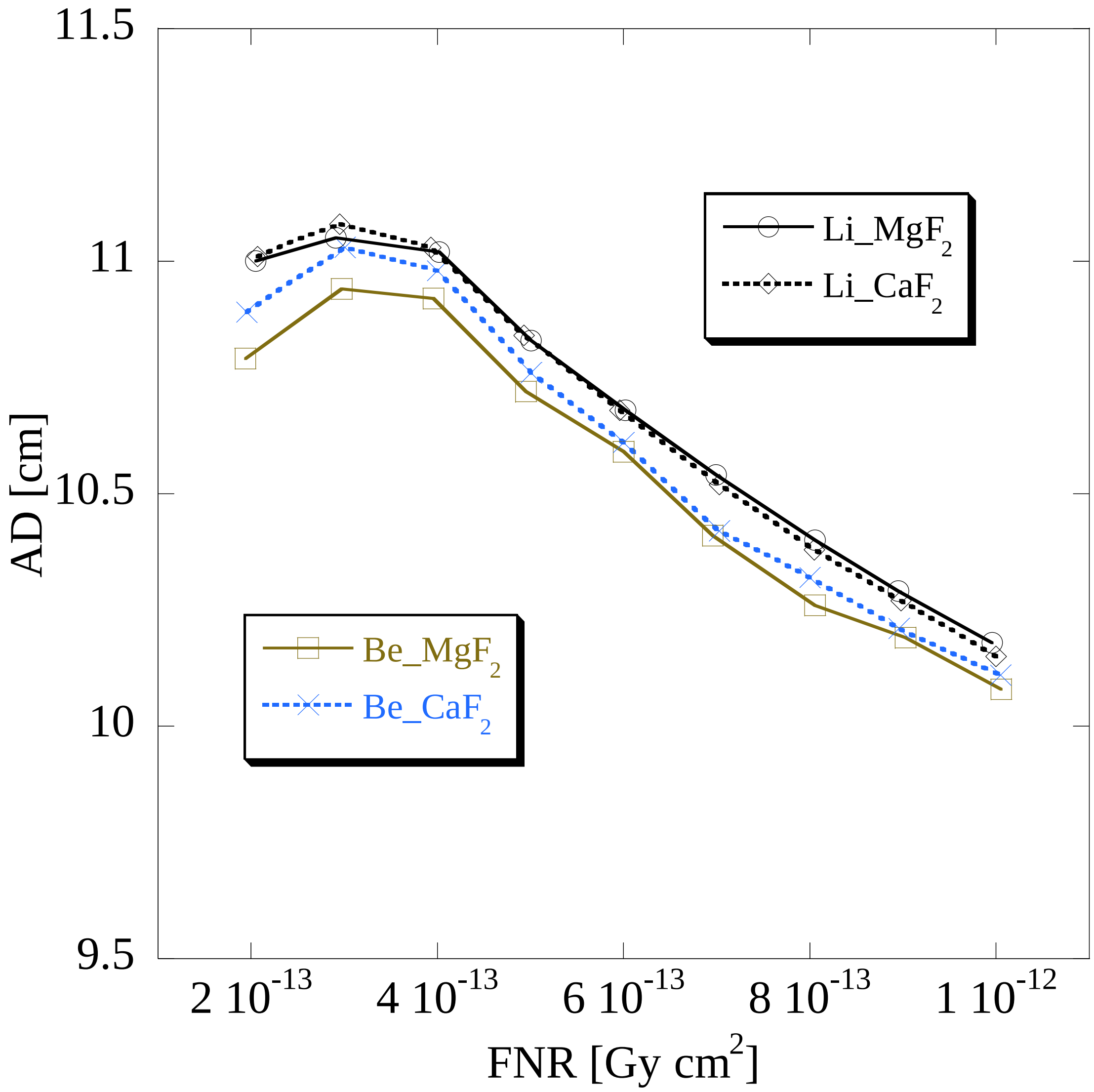

Fig. 6. Dependence on the FNR of the AD of the neutron beam for BSA models with a Li or Be target and a MgF_2 or CaF_2 moderator when $T/N = 100$ ($T = 65$ ppm, $N = 0.65$ ppm)

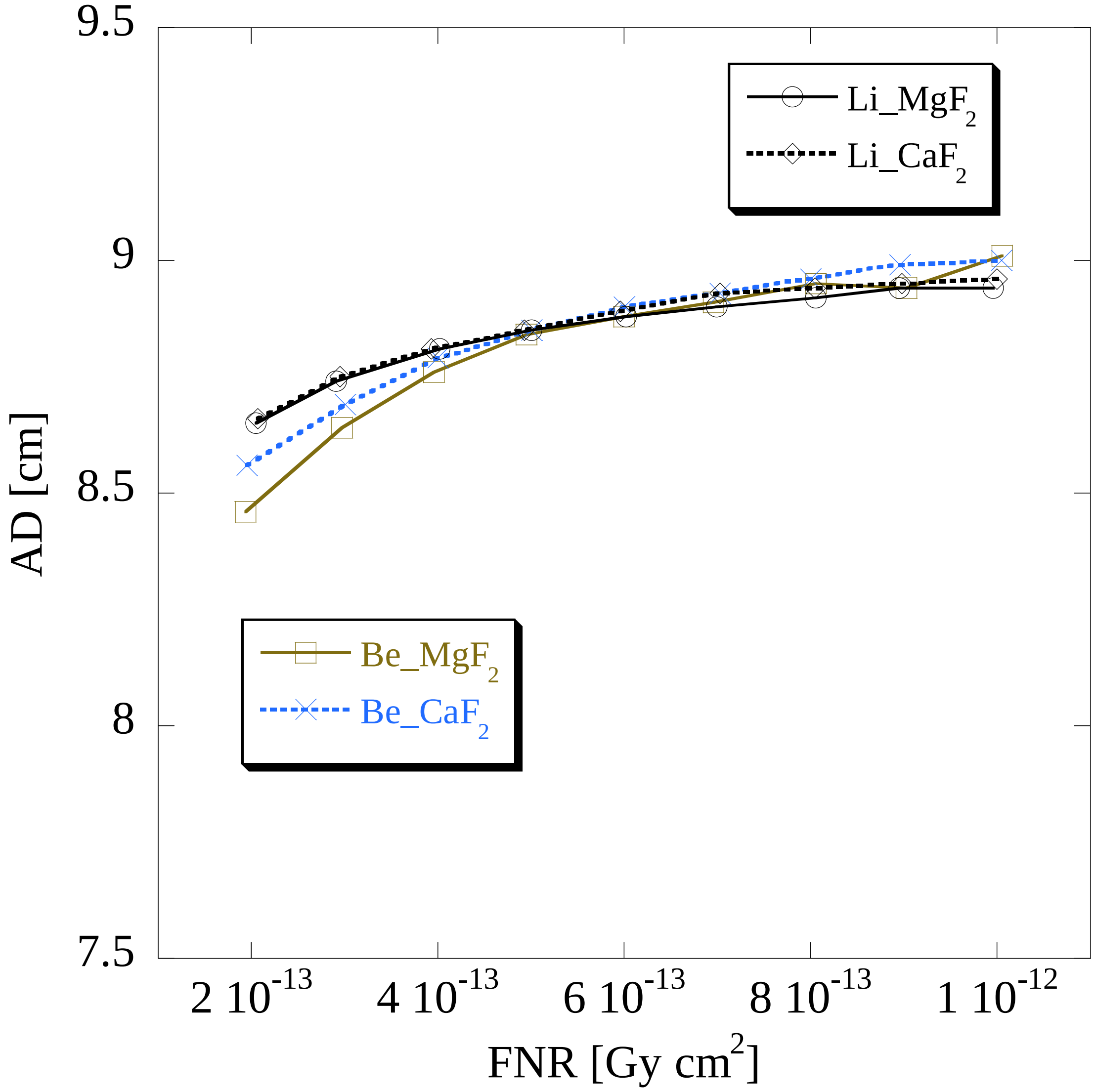

Fig. 7. Dependence on the FNR of the AD of the neutron beam for BSA models with a Li or Be target and a MgF_2 or CaF_2 moderator when $T/N = 3.61$ ($T = 65$ ppm, $N = 18$ ppm)

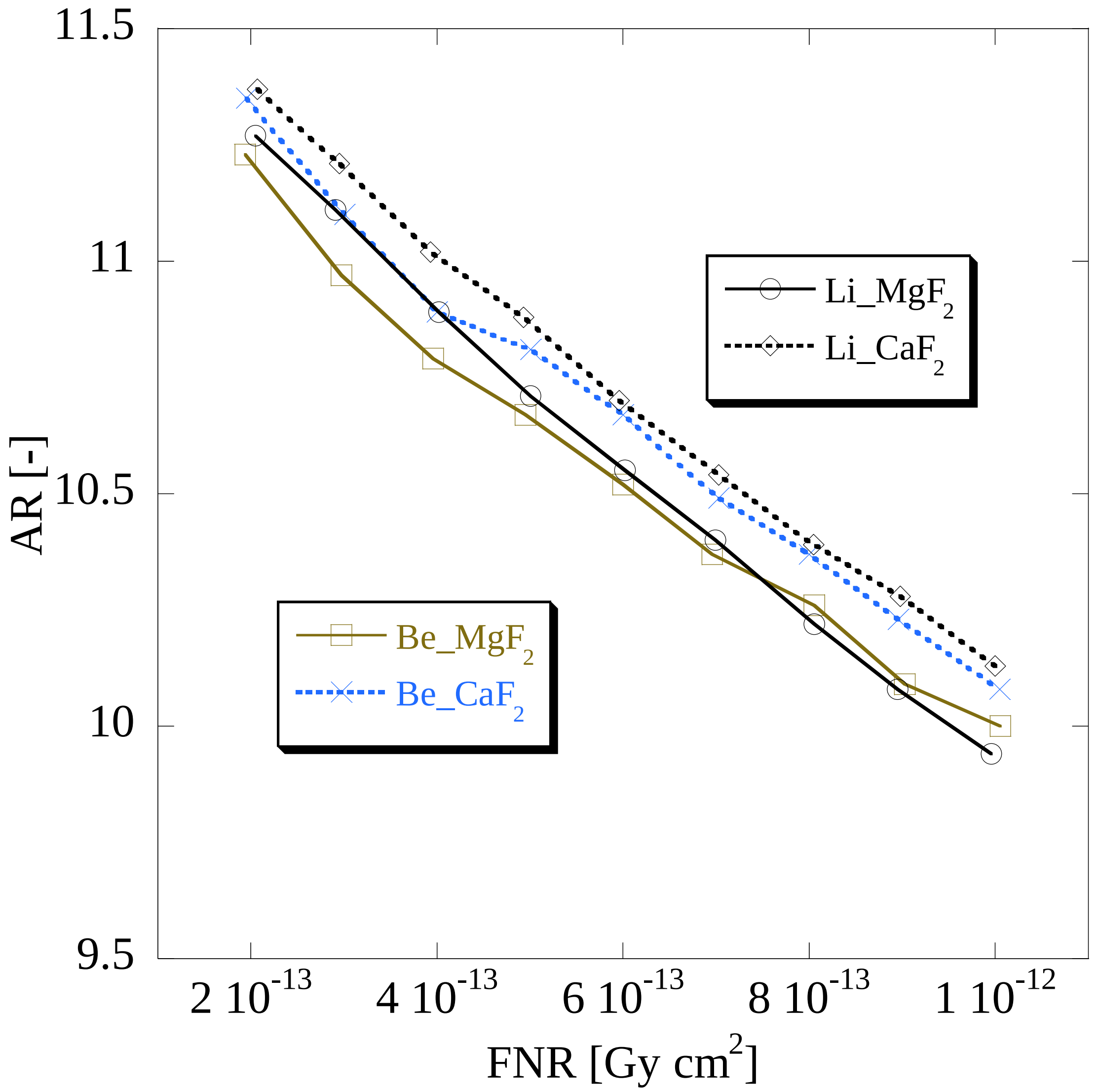

Fig. 8. Dependence on the FNR of the AR of the neutron beam for BSA models with a Li or Be target and a MgF_2 or CaF_2 moderator when $T/N = 100$ ($T = 65$ ppm, $N = 0.65$ ppm)

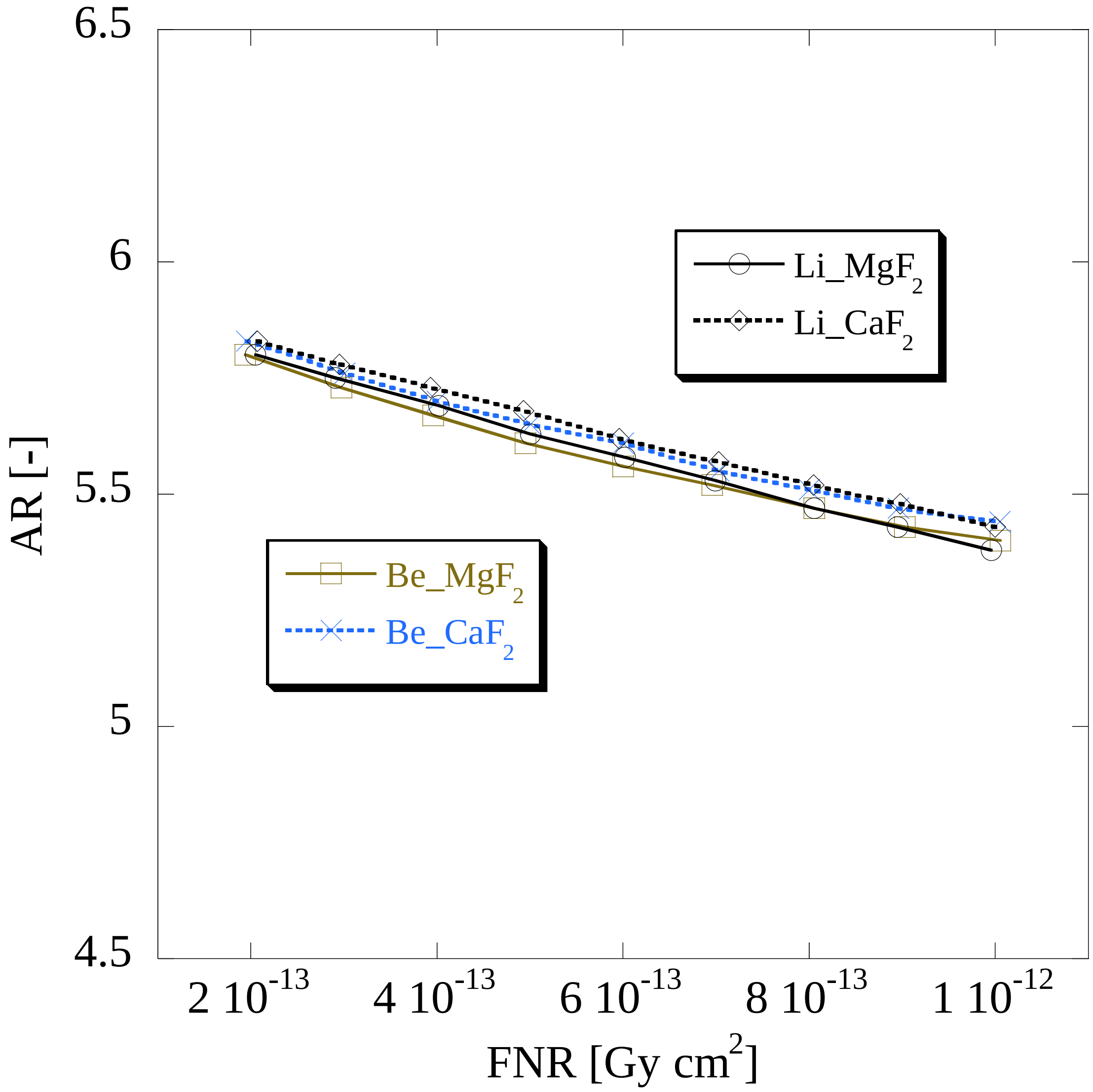

Fig. 9. Dependence on the FNR of the AR of the neutron beam for BSA models with a Li or Be target and a MgF_2 or CaF_2 moderator when $T/N = 3.61$ ($T = 65$ ppm, $N = 18$ ppm)

Table 1. Dependence of BSA characteristics and irradiation times (*IT*) on the FNR for a MgF_2 moderator and a Li target

FNR [× 10^{-13} Gy cm^2]	$T_{\mathrm{Li\_MgF_2}}$ [cm]	PHR [× 10^{-13} Gy cm^2]	TNR [×100]	J_T/φ_T	$\varphi_{\mathrm{Li\_MgF_2}}$ [× 10^9 cm^{-2}·s^{-1}]	$IT_{\mathrm{Li\_MgF_2}}$ [s], for *N* = 0.65 ppm	$IT_{\mathrm{Li\_MgF_2}}$ [s], for *N* = 18 ppm
2.05	27.2	0.96	1.84	0.626	1.38	2494.8	1226.3
2.91	24.8	0.86	1.78	0.627	1.58	2115.8	1050.0
4.02	22.7	0.78	1.73	0.628	1.76	1762.2	914.2
5.01	21.3	0.73	1.71	0.629	1.88	1466.1	830.8
6.02	20.2	0.71	1.69	0.630	1.98	1267.2	769.2
6.99	19.3	0.69	1.69	0.631	2.06	1117.1	719.7
8.06	18.5	0.66	1.68	0.631	2.12	991.7	677.3
8.95	17.9	0.66	1.68	0.632	2.18	906.0	647.5
9.96	17.3	0.65	1.68	0.633	2.22	828.4	617.4

Table 2. Dependence of BSA characteristics and irradiation times on the FNR for a CaF_2 moderator and a Li target

FNR [× 10^{-13} Gy cm^2]	$T_{\mathrm{Li\_CaF_2}}$ [cm]	PHR [× 10^{-13} Gy cm^2]	TNR [×100]	J_T/φ_T	$\varphi_{\mathrm{Li\_CaF_2}}$ [× 10^9 cm^{-2} s^{-1}]	$IT_{\mathrm{Li\_CaF_2}}$ [s], for *N* = 0.65 ppm	$IT_{\mathrm{Li\_CaF_2}}$ [s], for *N* = 18 ppm
2.07	44.0	0.88	1.90	0.619	0.82	4329.0	2109.2
2.95	40.0	0.80	1.85	0.619	0.97	3511.9	1731.0
3.93	37.0	0.75	1.82	0.620	1.10	2884.3	1490.3
4.93	34.6	0.72	1.80	0.620	1.21	2339.9	1316.9
5.96	32.7	0.69	1.80	0.621	1.30	1961.2	1192.5
7.03	31.1	0.68	1.79	0.622	1.37	1676.2	1098.4
8.05	29.8	0.66	1.79	0.622	1.44	1474.0	1021.4
8.98	28.8	0.65	1.79	0.622	1.48	1333.3	965.1
10.00	27.8	0.65	1.79	0.623	1.53	1200.1	910.8

Table 3. Dependence of BSA characteristics and irradiation times on the FNR for a MgF_2 moderator and a Be target

FNR [× 10^{-13} Gy cm^2]	$T_{Be\_MgF_2}$ [cm]	PHR [× 10^{-13} Gy cm^2]	TNR [×100]	J_T/φ_T	$\varphi_{Be\_MgF_2}$ [× 10^9 cm^{-2} s^{-1}]	$IT_{Be\_MgF_2}$ [s], for N = 0.65 ppm	$IT_{Be\_MgF_2}$ [s], for N = 18 ppm
1.94	27.1	1.08	2.08	0.614	1.34	2637.9	1292.5
2.97	20.3	0.78	1.89	0.614	1.90	1798.2	899.6
3.96	16.9	0.67	1.84	0.613	2.21	1424.7	759.6
4.95	14.7	0.64	1.82	0.613	2.42	1159.5	678.7
6.00	13.1	0.59	1.81	0.613	2.55	988.0	624.0
6.96	11.9	0.58	1.80	0.613	2.64	865.8	588.1
8.06	10.8	0.57	1.81	0.612	2.72	763.8	552.5
9.03	10.0	0.57	1.84	0.613	2.77	704.3	522.9
10.06	9.3	0.57	1.84	0.613	2.81	647.3	511.3

Table 4. Dependence of BSA characteristics and irradiation times on FNR for a CaF_2 moderator and a Be target

FNR [× 10^{-13} Gy cm^2]	$T_{Be\_CaF_2}$ [cm]	PHR [× 10^{-13} Gy cm^2]	TNR [×100]	J_T/φ_T	$\varphi_{Be\_CaF_2}$ [× 10^9 cm^{-2} s^{-1}]	$IT_{Be\_CaF_2}$ [s], for N = 0.65 ppm	$IT_{Be\_CaF_2}$ [s], for N = 18 ppm
1.95	39.1	0.91	1.98	0.615	1.05	3370.7	1646.4
3.01	31.5	0.77	1.87	0.615	1.45	2374.6	1175.8
4.00	27.0	0.69	1.84	0.614	1.72	1830.7	969.9
5.01	24.0	0.64	1.83	0.614	1.91	1478.6	854.1
6.00	21.5	0.62	1.82	0.614	2.07	1230.0	768.7
7.03	19.5	0.61	1.82	0.614	2.19	1037.0	704.9
8.00	18.0	0.58	1.82	0.613	2.28	923.4	661.8
8.96	16.7	0.58	1.83	0.613	2.36	835.2	623.4
10.05	15.5	0.57	1.83	0.613	2.42	754.5	592.0